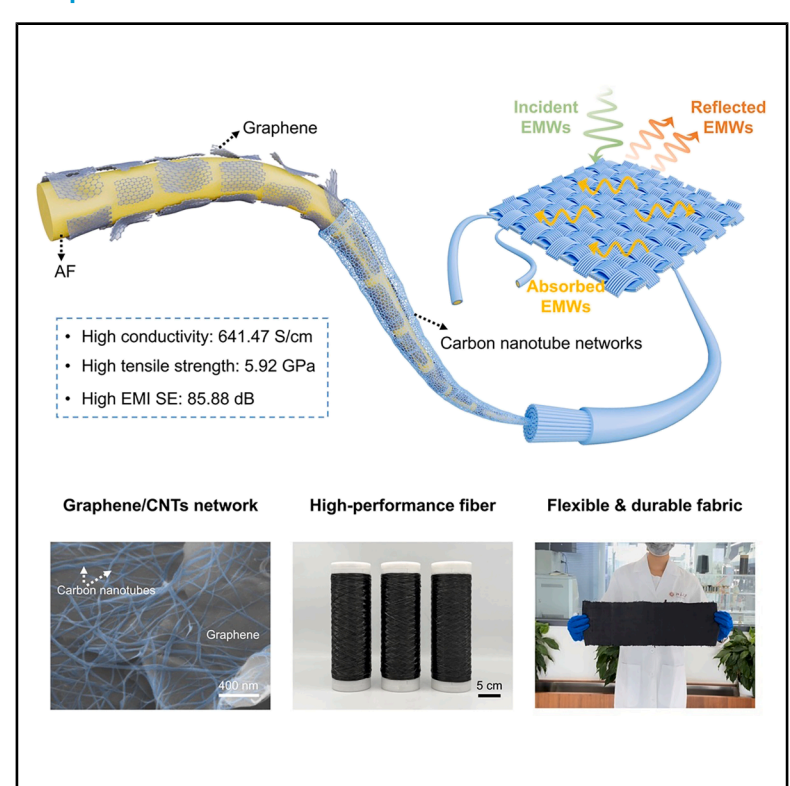
Dimension-engineered sequential assembly of carbonene materials on arbitrary fiber substrates for electromagnetic interference shielding

Graphical abstract



Authors

Jiayi Liu, Quanfen Guo, Huahui Tian, ..., Jiaxin Zheng, Jin Zhang, Xin Gao

Correspondence

gaoxin-cnc@pku.edu.cn

In brief

A dimension-engineered sequential assembly of graphene and CNTs yields robust coatings on diverse fibers, enabling durable, high-performance EMI shielding fabrics.

Highlights

- A dimension-engineered assembly strategy enables robust coatings on arbitrary fibers
- Coated fibers exhibit high conductivity while maintaining excellent tensile strength
- The resulting fabrics exhibit effective EMI shielding even under harsh conditions



Liu et al., 2025, Matter 8, 102427 October 1, 2025 © 2025 Elsevier Inc. All rights are reserved, including those for text and data mining, Al training, and similar technologies. https://doi.org/10.1016/j.matt.2025.102427



Matter



Article

Dimension-engineered sequential assembly of carbonene materials on arbitrary fiber substrates for electromagnetic interference shielding

Jiayi Liu, 1,2,3,7 Quanfen Guo, 1,2,7 Huahui Tian, 2,4,7 Yao Cheng, 2,7 Xianqi Xu,5 Ziyi Zhang, 1,2 He Hao,6 Zixuan Ding, 1,2,8 Kun Jiao, 1,2 Jiaxin Zheng, 5 Jin Zhang, 1,2,6 and Xin Gao 1,2,8,*

PROGRESS AND POTENTIAL Electromagnetic interference (EMI) shielding is essential in fields ranging from aerospace and defense to wearable electronics. Carbonene materials such as graphene and carbon nanotubes (CNTs) offer exceptional electrical and mechanical properties, making them ideal candidates for EMI shielding. However, scalable strategies for uniformly integrating these nanomaterials onto diverse fiber substrates remain limited. This work presents a dimension-engineered sequential assembly strategy that leverages the complementary geometries of two-dimensional graphene and one-dimensional CNTs to construct conformal, robust coatings on arbitrary fibers. The study underscores the critical role of dimensionality in guiding liquid-phase nanomaterial assembly. The resulting graphene/CNT-coated aramid fibers (GCAFs) exhibit high electrical conductivity and mechanical strength. When woven into fabrics, they deliver an average EMI shielding effectiveness of 85.88 dB and retain performance under harsh conditions. This strategy addresses key challenges in functional fiber manufacturing and offers a scalable, generalizable pathway toward lightweight, flexible, and high-performance EMI shielding textiles and composites.

SUMMARY

Carbonene materials such as graphene and carbon nanotubes (CNTs) exhibit exceptional electrical properties, making them promising for electromagnetic interference (EMI) shielding coatings. However, their hydrophobic and chemically inert nature poses challenges for uniform assembly onto hydrophilic or inert fiber surfaces, often requiring surface treatments or chemical modifications. Here, we report a dimension-engineering strategy to fabricate robust, conductive carbonene coatings on fiber substrates. Using a wet-chemistry assembly process, graphene sheets were first deposited as a base layer, followed by sequential integration of CNTs. This hierarchical assembly reduces graphene wrinkling and enhances sp^2 -carbon continuity. A 486-nm-thick carbonene coating boosted the conductivity of aramid fiber (AF) from 0 to 641.47 S/cm while maintaining a high tensile strength of 5.92 GPa. Fabrics woven from these coated AFs showed an EMI shielding effectiveness of 85.88 dB in the X band. This study presents an effective strategy for developing universal coatings, highlighting their applications for EMI shielding.

INTRODUCTION

The rapid development of fifth-generation wireless communication technology and electronic components has led to serious

electromagnetic interference (EMI) issues, which impact the security and stability of electronic devices. ^{1–4} EMI shielding technologies provide an effective solution to these challenges by attenuating electromagnetic wave (EW) propagation through



¹School of Materials Science and Engineering, Peking University, Beijing 100871, China

²Beijing Graphene Institute (BGI), Beijing 100095, China

³Academy for Advanced Interdisciplinary Studies, Peking University, Beijing 100871, China

⁴School of Chemistry and Chemical Engineering, Ningxia University, Yinchuan 750021, China

⁵School of Advanced Materials, Peking University, Shenzhen Graduate School, Shenzhen 518055, China

⁶Beijing Science and Engineering Center for Nanocarbons, Beijing National Laboratory for Molecular Sciences, College of Chemistry and Molecular Engineering, Peking University, Beijing 100871, China

⁷These authors contributed equally

⁸Lead contact

^{*}Correspondence: gaoxin-cnc@pku.edu.cn https://doi.org/10.1016/j.matt.2025.102427



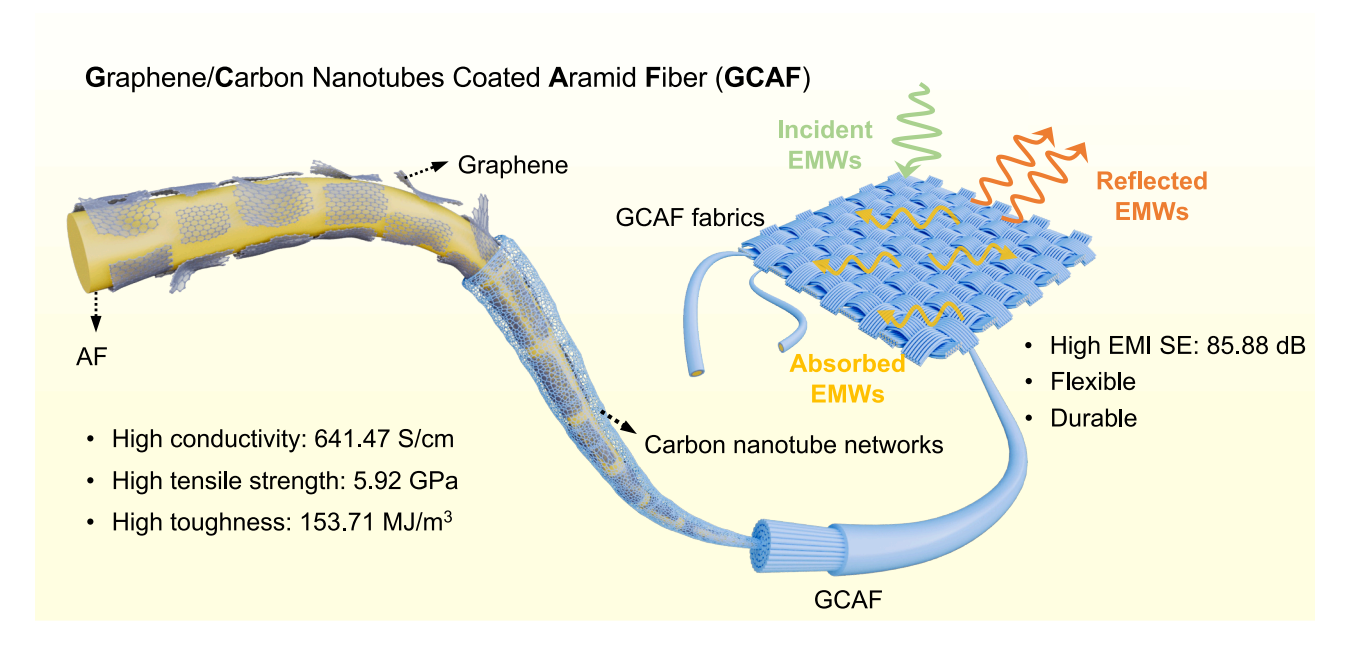


Figure 1. Schematic of the dimension-engineered assembly of carbonene materials onto aramid fibers for enhanced electromagnetic interference shielding

specialized shielding materials.5-7 To satisfy the stringent requirements of modern applications, next-generation EMI shielding materials are being developed with optimized characteristics including minimal thickness, broadband performance, mechanical robustness, and light weight, where advanced conductive nanomaterials are increasingly displacing traditional metallic alternatives.⁸⁻¹⁰ In this context, high-performance polymer fabrics with integrated EMI shielding capabilities have garnered significant attention. Their inherent flexibility, lightweight nature, and adaptability make them ideal candidates for emerging applications in aerospace, defense, and wearable electronics.1 enhance the electrical properties and thus enable the EMI shielding performance of these fabrics, direct surface modification techniques have been commonly employed. 15-17 However, fabrics prepared through such methods often suffer from issues like coating instability, poor breathability, and low conductivity.

Recently, a new direction has emerged to address these challenges by fabricating EMI shielding fabrics using conductive carbonene/polymer composite fibers. 18-21 Carbonene materials, such as graphene and carbon nanotubes (CNTs), are advanced carbon allotropes with exceptional electrical and mechanical properties, making them highly promising for EMI shielding applications. 22-24 Techniques such as direct spinning and surface dip coating have been employed to produce conductive carbonene/polymer composite fibers. 18,25,26 While spinning methods can achieve fibers with high conductivity and excellent EMI shielding effectiveness (SE), excessive use of conductive fillers often compromises the intrinsic mechanical properties of the fibers and fabrics. This results in materials with reduced strength and toughness and limited practical applicability. Surface dip coating has emerged as an efficient strategy to fabricate conductive carbonene/polymer composite fibers with high

strength by assembling carbonene materials from dispersions onto polymer fiber surfaces. ^{27,28} However, the assembly of hydrophobic and chemically inert carbonene materials onto hydrophilic or inert fiber surfaces typically requires surface treatments or chemical modifications. ^{29–31} These processes often involve complex fabrication steps and lead to increased impurity content, posing challenges to the scalability and performance of the final materials.

Here, we present a dimension-engineering strategy to fabricate universal carbonene coatings with exceptional mechanical stability and tunable conductivity on a variety of fiber substrates, including high-performance polymer and inorganic fibers. The coating process begins with the deposition of two-dimensional graphene nanosheets onto the fiber surface, forming a robust layered foundation. This is followed by the application of onedimensional CNTs, which wrap and compress the graphene, ensuring complete sp^2 -carbon coverage on the fiber surface. As a model system, we selected aramid fiber (AF), a widely used high-performance polymer fiber, as the substrate (Figure 1). This approach enabled the successful development of graphene/CNT-coated AF (GCAF) without compromising the intrinsic properties of the fiber or introducing foreign impurities. The GCAF exhibits remarkable conductivity, reaching 641.47 S/cm with a coating thickness of only 486 nm while maintaining an impressive tensile strength of 5.92 GPa. Notably, its conductivity surpasses that of Toray T700S carbon fibers. Moreover, the functional fabric woven from GCAF (GCAF fabric [GCAFF]) demonstrates exceptional EMI shielding performance, achieving an average SE of 48.64 dB in the X band for a single layer with a thickness of 0.42 mm. This performance increases to 85.88 dB with three layers, corresponding to nearly 100% SE. The GCAFF maintains its EMI shielding performance under extreme



conditions, including exposure to fire, washing, bending, and twisting. Additionally, the flexible and conductive GCAFF exhibits excellent electric heating capabilities. At an applied voltage of 12 V, the surface temperature of the GCAFF stabilizes at 225°C with a uniform temperature distribution, even after 180° bending. Our finding highlights the critical role of dimensional effects in the liquid-phase assembly of nanomaterials, and we propose an effective strategy for developing multifunctional EMI shielding fabrics that integrate structural and functional performance.

RESULTS

Preparation and characterization of GCAF

The preparation process of GCAF is illustrated in Figure S1, utilizing a two-step dip-coating strategy. Initially, graphene nanosheets are deposited onto the surface of AFs through dip coating in a graphene dispersion, followed by roller-press drying. The graphene nanosheets adhere to the fiber surface via van der Waals forces and π - π interactions between the graphene and AFs,³² resulting in graphene-coated AFs (GAFs). Subsequently, CNTs are applied to the surface of the GAFs using a similar dip-coating method, forming a stable and uniform CNT coating. The AF-G-CNT-layered structure offers several advantages: (1) graphene nanosheets alone face challenges in forming a tight and uniform coating on the smooth and inert cylindrical fiber surface. However, the cross-linked CNT network on the outer layer effectively binds and anchors the graphene sheets to the fiber surface, ensuring stability. (2) CNTs interconnect adjacent graphene nanosheets, serving as conductive bridges that create a continuous and stable conductive network. This synergistic interaction significantly enhances the overall conductivity of the structure.

The above two steps utilize a self-designed automated dip coater: on one side, the fibers are unwound and fed into an immersion bath containing the dispersion. They then pass through a drying unit equipped with infrared lamps and are finally rolled up on the other side. It is worth noting that both the immersion bath and the drying unit are equipped with four rollers. The rollers in the immersion bath facilitate the movement of the fibers along the designated trajectory under a controlled shear tension, ensuring adequate coating. In the drying unit, the rollers apply pressure to the fibers during the drying process, enhancing the adhesion between the substrate and the skin. This setup enables continuous and efficient preparation of the GCAF. At a coating speed of 20 m/min using a 12,000D AF substrate, the estimated production capacity of the GCAF reaches approximately 10.45 kg per day. To achieve the high electrical conductivity of the fibers, the quality of graphene and CNT dispersions is essential. The dispersions of graphene and CNTs were obtained through ultrasonic dispersion facilitated by surfactants (Figure S2). Optical microscopy showed that both graphene and CNTs exhibited improved dispersion uniformity when sodium dodecyl sulfate (SDS) was used as a dispersant, with optimal dispersions observed at mass ratios of 1:1 for graphene to SDS (Figure S3) and 2:5 for CNTs to SDS (Figure S4). We characterized the morphology and size of the graphene and CNTs by transmission electron microscopy (TEM) (Figure S5). The TEM images revealed the high aspect ratio of the single-walled CNTs, with an average length of 11.9 μ m, which is critical for enhancing electron transport along the tube's axial direction. The graphene sheets displayed a few-layer structure with large lateral dimensions, averaging 3.92 μ m in diameter, which is advantageous for ensuring high electrical conductivity (Figure S6). Moreover, X-ray photoelectron spectroscopy (XPS) analyses revealed that the CNTs and graphene exhibited high C/O atomic ratios of approximately 11.7 and 24.7, respectively (Figure S7), indicating their low defect level. 32,33

Figure 2A shows a photograph of the GCAF. The typical morphology of GCAF after two graphene dip-coating cycles and six CNT dip-coating cycles (G2/C6) is presented in Figure 2B. The coated fiber exhibits a uniform surface with a diameter of approximately 13.12 \pm 1.28 μ m. The cross-sectional image of G2/C6 (inset of Figures 2B and S8) reveals the conformal attachment between the substrate and the coating, with a coating thickness of 486 nm. Additionally, the optical images and morphologies of the coated quartz fiber and the coated poly(p-phenylene-2,6-benzobisoxazole) (PBO) fiber, fabricated using the same process, are shown in Figures S9 and S10, respectively. The successful coating on both quartz fibers and PBO fibers underscores the versatility and universality of the dimension-engineered assembly strategy for carbonene materials on various fiber substrates. Figure 2C shows the Raman spectra of AFs, G2, and G2/C6. In addition to the characteristic peaks of the AF,34 the G and 2D modes of the graphene and CNTs are clearly observed in the Raman spectra of G2 and G2/C6, confirming the successful loading of graphene.³⁵ For G2/C6, the I_G/I_D ratio is approximately 24, indicating the low defect level of graphene and CNTs in the coating layer.

To investigate the interaction between carbonene materials and AFs, the theoretical binding energies among graphene sheets, CNTs, and the fiber substrate were calculated using density functional theory (DFT) (Figures S11 and S12). The calculated binding energies were -0.012 eV/Å² for graphene/AF, -0.0082 $eV/Å^2$ for CNTs/AF, and $-0.011 eV/Å^2$ for graphene/CNTs. The relatively higher binding energy between graphene and the AF substrate supports the use of graphene as the primer coating layer. In this configuration, CNTs can effectively cross-link adjacent graphene nanosheets through van der Waals forces and π - π stacking interactions, thereby reinforcing the structural integrity of the sequential assembly. Scanning electron microscopy (SEM) images from different graphene coating cycles reveal that, after one coating cycle, the sp²-carbon coverage is insufficient, with large gaps between graphene sheets hindering electron transfer (Figure 2D). Conversely, excessive coating cycles cause graphene sheets to stack, preventing close adhesion to the fiber surface and leading to eventual detachment (Figure S13). Consequently, two coating cycles were identified as optimal, achieving the highest coverage of graphene nanosheets on the fiber surface (Figure 2E). However, the graphene nanosheets on the fiber remain curled and unstable, likely due to the following reason. As illustrated in Figure S14, during the drying process, the evaporation of the solvent leads to the disappearance of capillary forces, causing the graphene sheets to curl.³⁶ To enhance the performance and stabilize the graphene

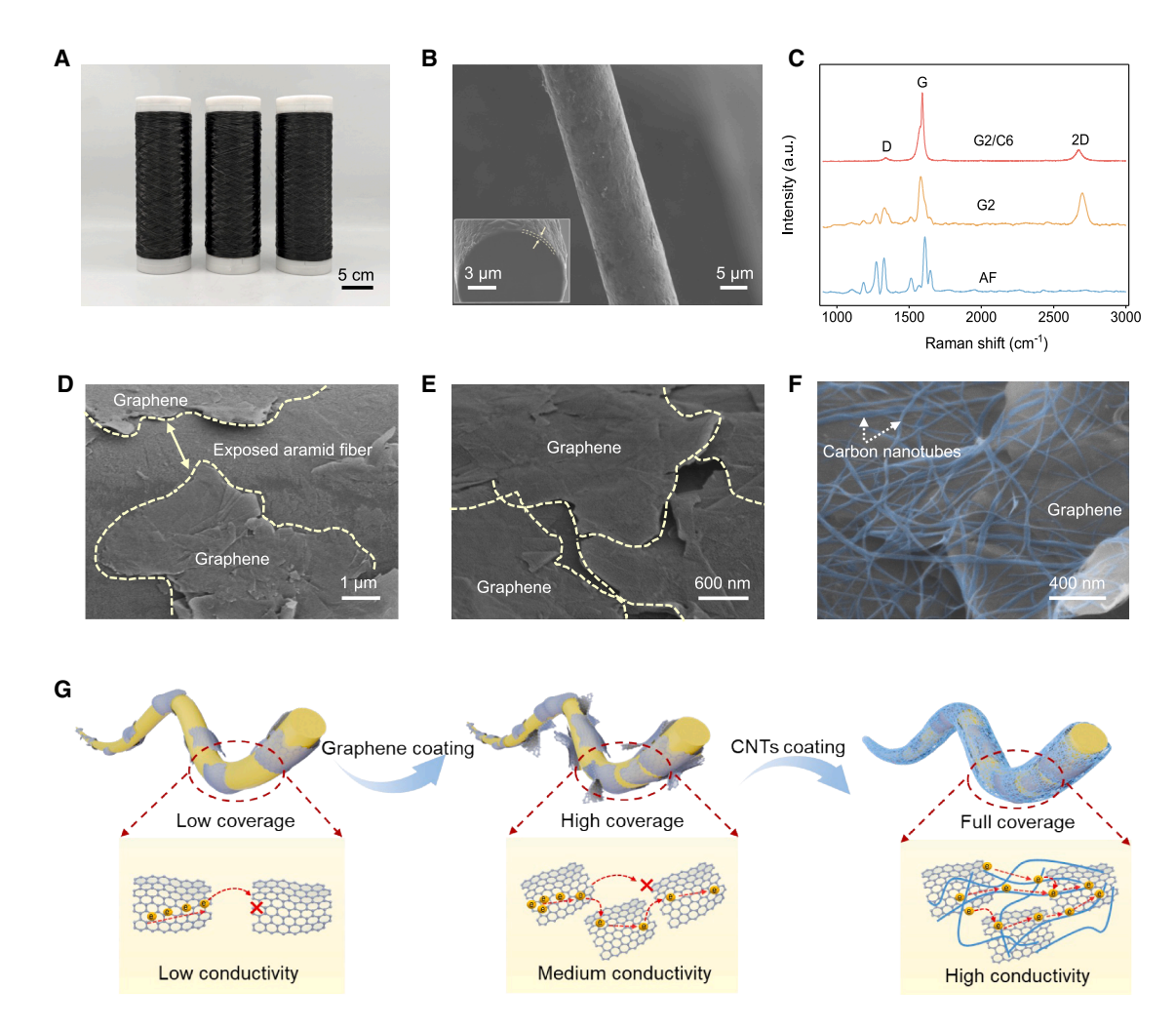


Figure 2. Characterizations of GCAFs

- (A) The photograph of GCAF.
- (B) The SEM images of GCAF. The left insets show the SEM image of the GCAF cross-section.
- (C) Raman spectra of AF, G2, and G2/C6.
- (D) The SEM image of G1.
- (E) The SEM image of G2.
- (F) The SEM image of G2/C6.
- (G) Electronic transport mechanism of different GCAFs. G1, G2, and G2/C6 represent AFs after one graphene dip-coating cycle, two graphene dip-coating cycles, and two graphene dip-coating cycles followed by six CNT dip-coating cycles, respectively.

coating, an additional CNT coating was applied. Increasing the number of CNT coating cycles led to a higher entanglement density of CNTs on the fiber surface, thereby enhancing the physical entrapment and stabilization of the graphene nanosheets (Figure S15). However, excessive dip-coating cycles may cause fiber stickiness, which could compromise processability and overall performance. After six CNT coating cycles, the sp^2 -carbon coverage on the fiber surface reached 100%, with a well-formed CNT network structure clearly observed (Figure 2F). The sp^2 -carbon coverage area on the fiber is directly linked to the electron transport mechanism of the carbonene materials within the coating layer, as illustrated in Figure 2G. Specifically, with a low coverage area, electron transport is limited by a huge poten-

tial barrier between the neighbors. As the coverage area increases, the distances between neighbor sheets decrease, yet electron transport still faces some barriers, resulting in relatively low mobility. Additional CNT coating increases the $sp^2\text{-}\mathrm{carbon}$ coverage area to nearly 100%, significantly reducing the energy barrier for carrier transport. The linear density was measured to assess the carbonene content of the fibers (Figure S16). The linear density of G2/C6 is 113.6 tex, which corresponds to a carbonene loading of 9.77 wt %, even lower than that of C8 (11.64 wt %). Tex, a unit widely used in the fiber industry, is the linear density in g/km. Therefore, the superior electrical conductivity of G2/C6 can be attributed to the more efficient conductive network design rather than a higher carbonene content.



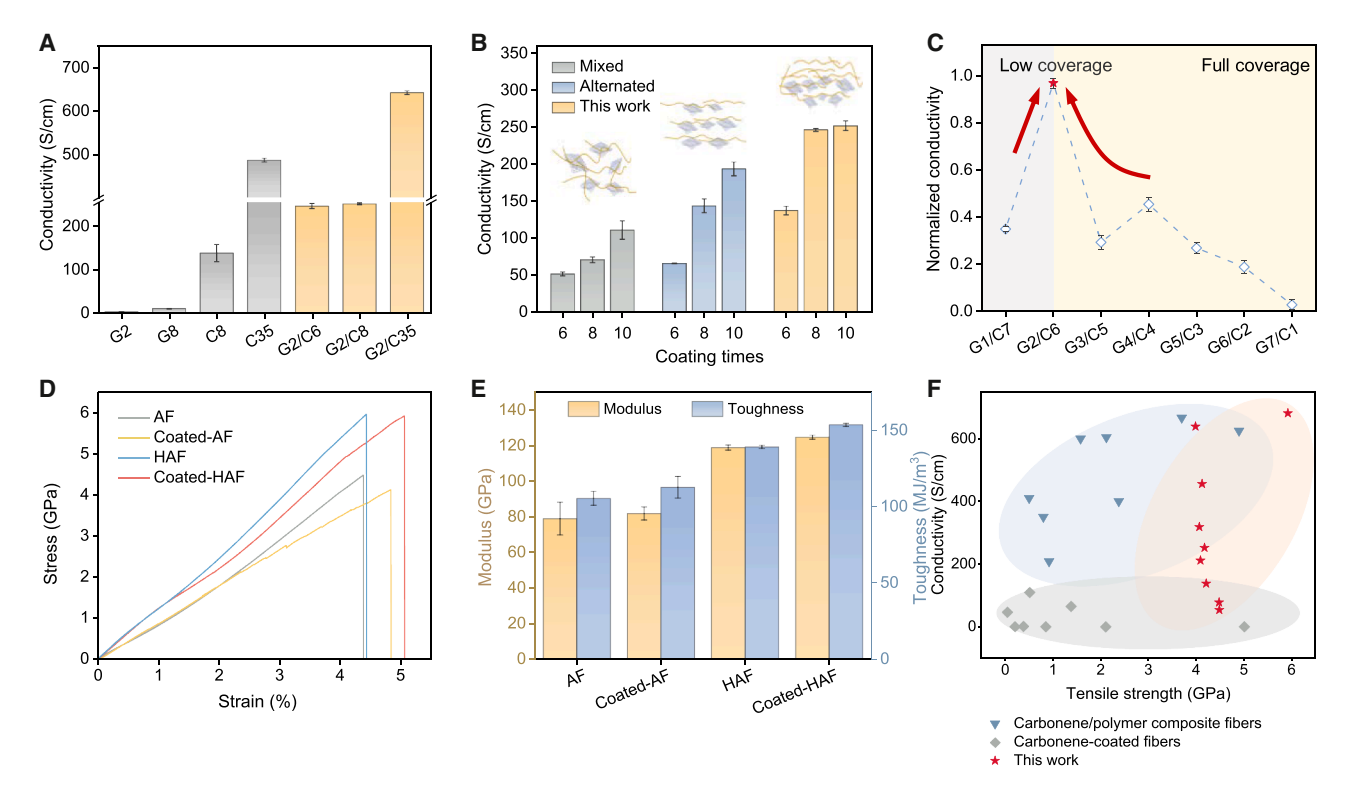


Figure 3. Electrical and mechanical properties of GCAFs

- (A) Electrical conductivity of different fibers.
- (B) Comparison of electrical conductivity of fibers prepared using different coating methods.
- (C) Normalized conductivity of different fibers with 8 coating cycles.
- (D) Stress-strain curves of different fibers.
- (E) Comparison of the Young's modulus and toughness of different fibers.
- (F) Comparison of electrical conductivity and tensile strength of different carbonene composite fibers and GCAF. See Table S1 for details.

MECHANICAL AND ELECTRICAL PROPERTIES OF GCAF

We further evaluated the electrical and mechanical properties of as-prepared GCAF. The electrical conductivity of fibers was calculated from the resistance measured using a digital source meter by a standard two-probe method (Figure S17). As shown in Figure 3A, after twice graphene coating, the G2 fiber exhibited an electrical conductivity of 2.38 S/cm. After further integration of CNTs, as the sp^2 -carbon coverage area increased, the conductivity of the GCAF improved significantly. The G2/C6 fibers exhibited a higher conductivity of 246.06 S/cm compared to graphene- (G8: 9.93 S/cm) and CNT- (C8: 137.91 S/cm) coated fibers, despite having the same number of dip-coating cycles. The conductivity of G2/C35 reached 641 S/cm, surpassing that of commercial Toray T700S carbon fibers. The tunability of the conductivity, ranging from 2.38 to 641.47 S/cm (Figure S18), makes it suitable for a wide range of practical applications.

To directly observe the charge distribution on the fiber surfaces, we measured the surface potential of the fibers by Kelvin probe force microscopy (KPFM). As shown in Figure S19A, after applying voltage to the conductive probe, the surface potential can be obtained through the electrostatic interaction between the probe tip and the surface charge of the fiber. We scanned the samples within a 4 \times 4 μm range, and the comparison of the

potential mapping shown in Figures S19B-S19D reveals a proaressive increase in conductivity from G8 to C8 to G2/C6.38 In addition, the electrical conductivity of fibers with different coating architectures is shown (Figure 3B). Various coating sequences involving graphene and CNTs were applied. The mixed graphene/CNT coating resulted in nonuniform and incomplete surface coverage on the AF (Figure S20), yielding a relatively low conductivity of 70.40 S/cm after 8 dip-coating cycles. An alternating coating strategy using separate graphene and CNT dispersions produced a higher conductivity of 143.31 S/cm under the same conditions. Remarkably, the GCAF fabricated via the dimension-engineered sequential assembly strategy demonstrated the highest electrical performance, achieving a conductivity of 246.06 S/cm. These findings highlight the advantages of the dimension-engineered sequential assembly method, which enables a more effective combination of graphene and CNTs for enhanced performance. Figure 3C illustrates the contribution of graphene and CNTs to the enhancement of conductivity under the same number of coating cycles, with a carbon content of approximately 10 wt %. Notably, when the graphene coating cycle was reduced to one, the conductivity of G1/C7 showed a significant decrease compared to G2/C6, owing to the lower sp²-carbon coverage area. With complete coverage, G2/C6 demonstrated superior electrical performance compared to



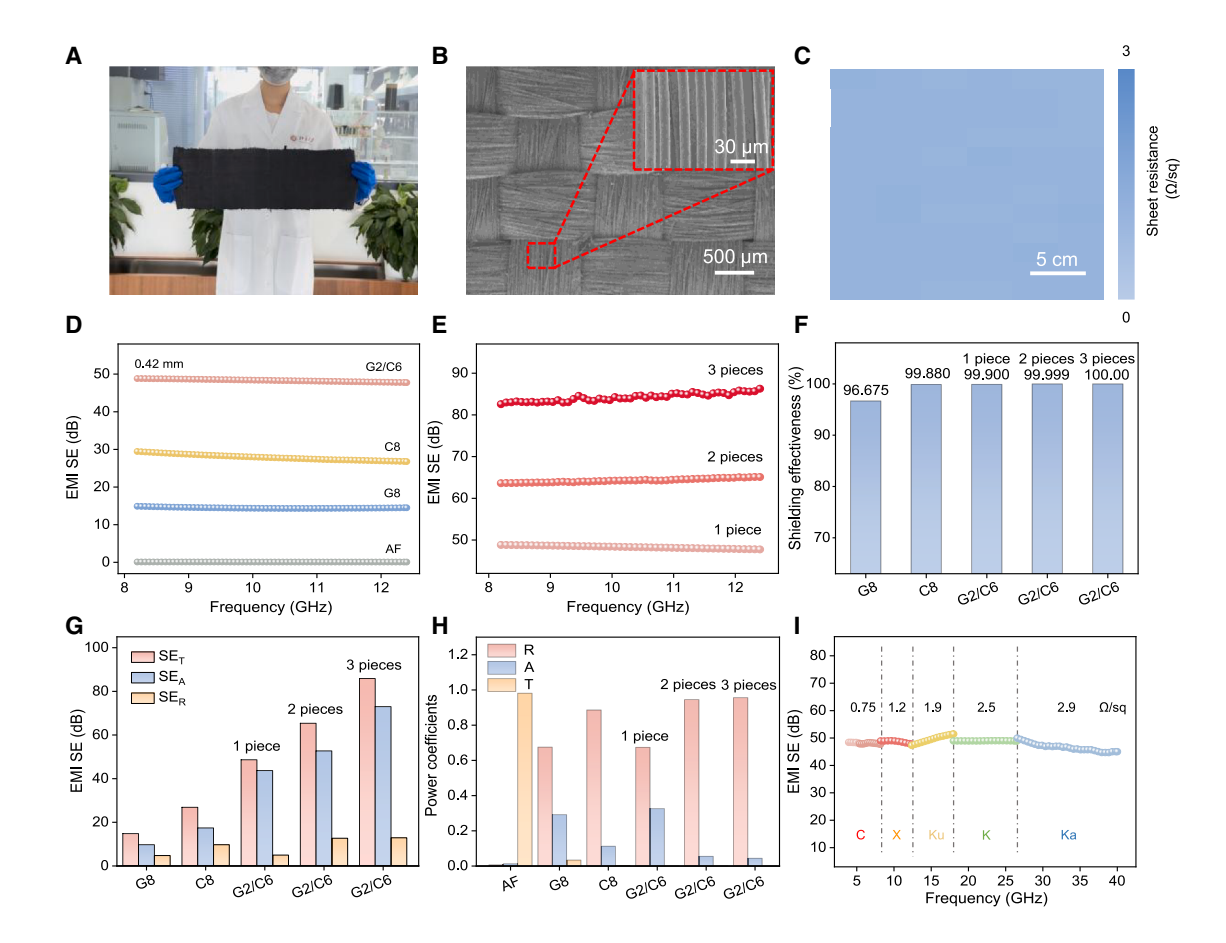


Figure 4. Characterizations of GCAFF and its EMI shielding properties

- (A) Photograph of GCAFF.
- (B) SEM image of GCAFF.
- (C) Sheet resistance mapping of GCAFF.
- (D) EMI SE_T of different fabrics in 8.2-12.4 GHz.
- (E) EMI SE_T of G2/C6 fabrics composed of 1-3 layers.
- (F) SE of different fabrics.
- (G) Average SE_T, SE_A, and SE_B of different fabrics.
- (H) Power coefficient A, R, and T values of different fabrics.
- (I) EMI SE_T of GCAFFs with different sheet resistances in 4–40 GHz.

other fibers, highlighting the importance of the base layer formed by two graphene coating cycles.

The stress-strain curve of the GCAF is shown in Figure 3D. For the G2/C6-coated AF, the tensile strength was \sim 4.21 GPa, with only a negligible change compared to the AF (\sim 4.32 GPa). Additionally, the network structure of the coating layer can release part of the stress during the deformation process^{39,40}; thus, the elongation at break, modulus, and toughness of the coated fiber are improved (Figures 3E and S21). Graphene oxide (GO)-enhanced heterocyclic AF (referred to as HAF) was also used as the fiber substrate for the universal carbonene assembly. The G2/C6-coated HAF exhibited excellent mechanical properties, with a tensile strength of 5.92 GPa, a toughness of 153.71 MJ/m³, a modulus of 124.82 GPa, and an elongation at break of 5.03%. Fractographic analysis of fibers after tensile testing revealed that coated AFs exhibited reduced fibrillation, with significantly fewer axial cracks extending along the fiber

axis (Figure \$23). This behavior is attributed to the strong interfacial adhesion between the coating and the fiber, which inhibits microfibril slippage during tensile loading. Overall, the as-prepared GCAF exhibited both tunable conductivity (ranging from 0 to 641.47 S/cm) and high mechanical strength (5.92 GPa), establishing it as a superior structural-functional integrated material. It outperforms most previously reported carbonene/polymer composite fibers and carbonene-coated fibers (Figure 3F; Table \$1).

EMI properties of GCAFF

High-strength, high-conductivity GCAF was woven into the GCAFF for EMI shielding applications. As shown in Figure 4A, a large area of fabric was obtained through the continuous weaving of G2/C6. The SEM image in Figure 4B reveals the interlaced structure of the GCAFF with aligned GCAFs (inset in Figure 4B). Sheet resistance measurements taken at 10 evenly



spaced positions on the GCAFF showed consistent values, confirming the uniformity of the coating (Figure S24, labeled A1–A10). The sheet resistance mapping image of the GCAFF showed a low surface resistance of $1.2 \pm 0.5 \,\Omega/\text{sq}$ (Figure 4C), highlighting its strong potential for EMI shielding.

The EMI SE of the GCAFF was measured using a vector network analyzer. As shown in Figure 4D, the AF fabric exhibited negligible EMI shielding performance, with a SE_T of almost 0 dB in the X-band range (8.2-12.4 GHz). After 8 dip-coating cycles of graphene dispersion (G8), the EMI SE improved, reaching a maximum SE_T of approximately 14.78 dB. The GCAFF coated with CNTs (C8) demonstrated even higher EMI SE, with a SE_T value of 26.87 dB, owing to the enhanced conductivity provided by the CNTs. With a more efficient conductive network on the fiber surfaces, the single-layer G2/C6 fabric exhibited excellent EMI SE performance with a SE_T of 48.64 dB at a thickness of only 0.42 mm. In comparison, the EMI SE of the mixed graphene-CNT-coated AF fabric was limited to 30.38 dB, primarily due to reduced conductivity-induced loss on the fabric surface (Figure S25). As shown in Figure 4E, the EMI shielding performance of the G2/C6 fabric improved with the addition of layers. When two and three fabric layers were stacked, the SE_T increased to 65.38 and 85.88 dB in the X band, respectively. These results demonstrate that a single-layer G2/C6 fabric can effectively block 99.9% of incident EWs (Figure 4F). With the increase in fabric layers to two and three, the SE further rises to 99.999% and nearly 100%, indicating extremely high SE. Due to the versatility of this dimension-engineered wet-chemistry assembly method, coated PBO fabric and coated quartz fabric also exhibited excellent shielding performance, achieving three-layer SE_T values of 64.28 and 70.64 dB, respectively (Figure S26).

Figure 4G shows the average value changes of SE_R and SE_A of fabrics in different layers woven by G8, C8, and G2/C6. The value of SE_T is the sum of SE_R and SE_A . The formation of a more efficient conductive network increased fiber conductivity; thus, the SE_R value of the fabric improved from 4.75 dB for G8 to 9.70 dB for C8. However, after adding the intermediate graphene layer, the average SE_R value of the G2/C6 fabric decreased to 4.95 dB, while the corresponding average SE_A value increased to 43.69 dB (Figure S27). This can be attributed to the addition of graphene, which reduced the surface potential while enhancing interfacial polarization (Figure S19). The layered structure formed by graphene and CNTs improved the multireflection of EWs at interfaces, enhancing the EW absorption induced by electric dipoles and interfacial polarization.

The power coefficients R (reflection), A (absorption), and T (transmission) were calculated using the S parameters to further explore the EMI shielding mechanism of the GCAFF (Figure 4H). The bare AF fabric exhibited the highest EW transparency, with 98.14% of EW energy transmitted through the fabric. In comparison, the EW energy transmitted through the G8 fabric was reduced to 3.34%, with the remaining 67% and 29% of the EW energy being reflected and absorbed, respectively. The increased conductivity of C8 leads to enhanced EW reflection at the fabric surface, resulting in a higher reflection coefficient (R) value of 0.89 and a lower absorption coefficient (A) value of 0.11. This indicates that C8-coated fibers are more effective at reflecting incident EWs, contributing to better EMI shielding per-

formance. Notably, compared to the G8 and C8 fabrics, a noticeable change in the shielding mechanism for the G2/C6 fabric is observed. The A value of the GCAFF rises to 0.33, while the R value drops to 0.67, demonstrating an improvement in absorption and a reduction in reflection, although reflection remains the dominant shielding mechanism. Due to the multi-interface structure of the graphene/CNT network, the inhomogeneity of the medium allows the multiple reflection of EWs at the interfaces, which is the primary reason for the improvement of the EW absorption and the weakening of the reflection. The EMI shielding mechanism of GCAFF is summarized in Figure S28. The GCAFF exhibit remarkable SE compared to previously reported carbonene-based shielding materials at low carbonene coating content (~9.77 wt %) (Figure S29; Table S2).

Additionally, we measured the EMI SE of fabrics with different surface resistances to evaluate the shielding performance of GCAFFs across the ultra-broadband frequency range of 4–40 GHz. As shown in Figure 4I, the 0.42-mm-thick GCAFFs, with average surface resistances of 0.75, 1.2, 1.9, 2.5, and 2.9 $\Omega/$ sq, respectively, maintain excellent EMI SE of $\sim\!\!48$ dB across the C, X, Ku, K, and Ka bands. This evaluation provides a comprehensive understanding of the fabric's ability to block EMI over a wide range of frequencies, demonstrating its potential for various practical applications in EMI shielding.

The application of GCAFF under harsh conditions

To evaluate the reliability of the GCAFF under harsh conditions, a series of tests was conducted after fire exposure, washing, and bending of fabrics. First, we subjected the GCAFF to external flame exposure from an alcohol lamp to simulate the harsh conditions of the fabric's exposure to fire. The results showed that after being continuously exposed for 60 s in both horizontal and vertical combustion environments, the fabric maintained a high shape retention rate (Figure S30). Figure 5A shows the changes in sheet resistance of the G2/C6 fabric at different combustion times. The sheet resistance of the as-prepared GCAFF stabilizes at a value of $R/R_0 = 2.86$ after 60 s, owing to the robust dimensionengineered coating layer. In contrast, the fabric with only a graphene coating shows a continuous increase in resistance, which is associated with the instability of the graphene layers during the combustion process. This demonstrates the enhanced stability and durability of the GCAFF due to the integrated graphene and CNT coating. The EMI shielding performance of the G2/C6 fabric was tested after burning for 20, 40, and 60 s, with SE_T values of 38.32, 37.09, and 35.23 dB, respectively (Figures 5D and S31A). With an SE (SE_T) \geq 20 dB indicating less than 1% EW transmission, 41 the fabric retains good shielding capability.

To evaluate the washing resistance of the fabric, we recorded the sheet resistance change of the fabrics over 12 washing cycles, each lasting 10 min (Figure 5B). After 12 washing cycles, the resistance of the G2/C6 fabric remains stable, with an R/R0 value of 1.06, and the structure on the fiber surface remains intact (Figure S32). In contrast, due to the weak adhesion of the graphene layers, the G8 fabric showed a clear increase in sheet resistance after washing. Similarly, the EMI SE value of the GCAFF after washing remains high at 43.75 dB (Figures 5E and S31B), which indicates the excellent stability and wash resistance of the GCAFF enabled by carbonene-coated fibers.

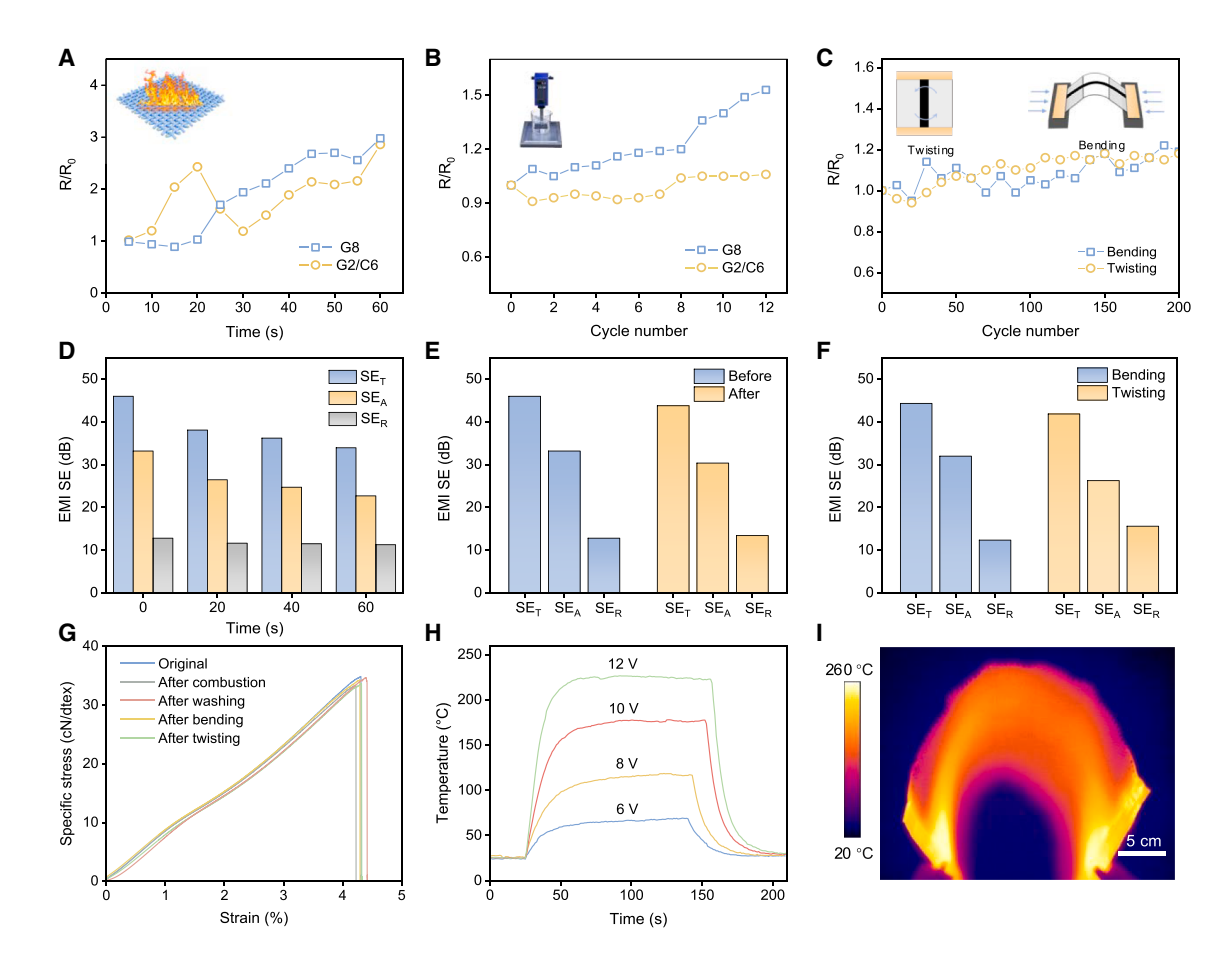


Figure 5. The electrical, EMI shielding, mechanical, and electric heating performance of GCAFF under harsh conditions

- (A) Sheet resistance changes over 60 s of burning.
- (B) Sheet resistance changes over 12 cycles of washing.
- (C) Sheet resistance changes over 200 cycles of bending and twisting.
- (D) EMI SE values after different burning times.
- (E) EMI SE values after different washing times.
- (F) EMI SE values after different bending and twisting times.
- (G) Specific tensile strength and modulus of GCAF yarns after burning, washing, bending, and twisting.
- (H) Time-dependent temperature variation of GCAFF under different voltages.
- (I) Infrared image of the GCAFF electrothermal device after 180° bending.

We further tested the sheet resistance and EMI SE of the GCAFF after bending and twisting to characterize the impact of external forces such as pulling, weaving, and friction. The fabric exhibited excellent durability after 200 cycles of bending and twisting, with an increase in sheet resistance of only about 10% (Figure 5C). The fluctuations in resistance during bending arose from slight misalignment and mechanical mismatch between the AF substrate and the coatings. The EMI SE value of the GCAFF after 200 continuous twist cycles is 43.87 dB (Figures 5F and S31C), reflecting a modest decrease of 6.5% from the initial value. This slight decline can be attributed to the increased porosity and fraying of the fabric after twisting, which allows EWs to transmit to the backside. However, the total shielding value after bending remains at 45.04 dB, showing virtually no decline. The mechanical properties of the GCAFF treated under different harsh conditions are shown in Figure 5G. The specific

strengths of the G2/C6-coated HAF yarns after combustion, washing, bending, and twisting are 32.51, 34.52, 34.22, and 33.57 cN/dtex, respectively, demonstrating only a slight decrease from the original strength of 34.87 cN/dtex. To further evaluate the durability, the GCAF yarns were subjected to 100 cycles of cyclic tensile testing under a constant tensile force of 150 N. After 100 cycles, the GCAF exhibited only slight changes in strain and conductivity (Figure S33), indicating the good mechanical and electrical stability of the coating. These results indicate the excellent durability of the GCAFF, highlighting its resilience under various environmental stresses.

The flexible conductive GCAFF also presented excellent electric heating capabilities. It can be used as an anti-icing heater, resisting ice and frost under extreme cold conditions. Figure 5H illustrates the typical heating and cooling curves of the flexible GCAFF heater under different applied voltages (6, 8, 10, and



12 V). The fabric demonstrated a rapid heating rate, reaching peak temperatures within 20 s, and maintained a stable surface temperature across all applied voltage levels. Furthermore, a strong linear relationship between the square of the applied voltage and the surface temperature (Figure S34) confirms that the electric thermal conversion performance complies with Joule's law. 42 It can be observed that, at an applied voltage of 12 V, the surface temperature of the GCAFF remained at 225°C, with a uniform temperature distribution even after 180° bending (Figure 5I). This indicates the excellent electrothermal performance, flexibility, and coating stability of the GCAFFbased heater. Furthermore, the GCAFF exhibited excellent air permeability (39.3 mm/s) and water vapor transmission rate (812.2 g m⁻² day⁻¹), as confirmed by the gas release experiment (Figure S35). Its porous structure allows HCl gas to diffuse into the air, where it reacts with NH₃·H₂O to produce a large amount of white smoke-like NH₄Cl. In contrast, the fabric coated with graphene and CNTs directly forms a continuous carbonene film on the fabric surface, which reduces its porosity and prevents the formation of white smoke, consequently leading to poor air permeability (4.6 mm/s) and water vapor transmission rate (160.8 g m $^{-2}$ day $^{-1}$).

DISCUSSION

In summary, we propose a dimension-engineering strategy to develop universal carbonene coatings with exceptional mechanical stability and tunable conductivity on various high-performance fiber substrates through a facile wet chemical method. The coating process involves the deposition of two-dimensional graphene nanosheets onto the fiber surface to form a layered foundation, followed by the application of one-dimensional CNTs to wrap and compress the graphene, ensuring complete sp²-carbon coverage. Using this strategy, a high-strength (5.92 GPa) and high-conductivity (641.47 S/cm) GCAF was successfully fabricated by coating graphene and CNTs onto the AF. In this design, CNTs interconnect the graphene sheets and serve as conductive bridges, forming a continuous and stable threedimensional conductive network. This unique structure imparts the GCAFF with an outstanding EMI SE of up to 48.64 dB in the X band for a single 0.42-mm-thick layer while maintaining high durability under various environmental conditions. These findings provide valuable insights into the scalable production of lightweight, structural-functional integrated EMI shielding fabrics with high strength, excellent conductivity, and superior environmental stability.

METHODS

Materials

Dimethylacetamide (DMAC; Macklin, \geq 99%), lithium chloride (LiCl; Macklin, >99%), 2-(4-aminophenyl)-1H-benzimidazol-5-amine (PABZ; Macklin, \geq 99.5%), terephthaloyl chloride (TPC; Macklin, \geq 99%), p-phenylenediamine (PPD; Macklin, \geq 99%), DABA-Cl (Macklin, \geq 99%), lauryl sodium sulfate (SDS, Aladdin, \geq 99%), and sodium dodecyl benzene sulfonate (SDBS; Aladdin, \geq 99%) were purchased from suppliers. The raw graphene, GO, and CNTs were procured from Deyang Carbonene Technology

and Nanjing XFNANO Materials Tech, respectively. The fiber substrate used in this study is para-AF.

Preparation of graphene dispersion

A specific amount of surfactant (SDS or SDBS) was dissolved in 200 mL of deionized water and subjected to ultrasonic treatment for 5 min to obtain a homogeneous solution. Then, 1.6 g graphene was added to the surfactant solution with subsequent ultrasonication for 1 h in an ice water bath using an Ultrasonic Cell Disruption System with 60% power (1,500 W) to achieve graphene dispersion. Herein, the concentration of graphene dispersion is 8 mg/g. Different mass ratios of surfactant to graphene (1:1, 1:2, and 2:1) can be obtained by adjusting the amount of surfactant added.

Preparation of CNT dispersion

The dispersion of CNTs followed a similar process to the preparation of graphene dispersion but with a concentration of CNTs of 2 mg/g. Different mass ratios of surfactant to CNTs (5:2, 2:1, and 3:1) were obtained by adjusting the amount of surfactant added.

Preparation of HAF through wet spinning

The HAF spinning dope was synthesized under a nitrogen (N_2) atmosphere by first dissolving PABZ, PPD, and DABA-CI in a DMAC/LiCl solution, followed by the dispersion of GO into the same solvent system. ⁴³ Polymerization was initiated by the addition of TPC, and the reaction mixture was stirred at 10° C for 1.5 h. After defoaming, the spinning solution was extruded through a spinneret into a series of coagulation baths with varying DMAC/ H_2 O compositions (50 wt % DMAC/50 wt % H_2 O and 20 wt % DMAC/80 wt % H_2 O). The as-spun fibers were subsequently washed, thermally treated at 400° C, and collected via winding.

Preparation of GCAF

The preparation of GCAF was carried out using an automatic dip-coating device. First, the AF was immersed in graphene dispersions to obtain GAF. The details of this process utilizing the dip-coating device are as follows: the wound AF was secured on one side of the device and pulled out. After passing through an immersion bath (1 m long and equipped with two internal rollers) containing graphene dispersions under specific stretching ratios, the soaked fibers were dried and subjected to a thermal roller pressing treatment at 260°C. Next, the GAF was immersed in CNT dispersions. A similar procedure was followed, in addition to replacing the immersion bath with a dispersion of CNTs. Finally, the GCAF was collected by winding.

Characterization

SEM images were collected from a Hitachi S4800 SEM, and the acceleration voltage was 5 kV. The radial cross-section of fibers was cut by a focused ion beam (FIB) (ZEISS Crossbeam 550). XPS was recorded using an Axis Ultra spectrometer with AI K α (1,486.6 eV) as the X-ray source. TEM images were performed on a FEI Tecnai F30 electron microscope operating at 300 kV. The optical images were taken with an LV100ND microscope (Nikon). Raman spectra of the fibers were obtained on a LabRAM HR Evolution system (Horiba, Japan) equipped with a laser





excitation wavelength of 532 nm (beam spot of $\sim\!\!1~\mu m).$ KPFM images were measured with a Dimension Icon microscope (Bruker). Detailed methods of characterization can be found in the supplemental information.

RESOURCE AVAILABILITY

Lead contact

Requests for further information and resources should be directed to and will be fulfilled by the lead contact, Xin Gao (gaoxin-cnc@pku.edu.cn).

Materials availability

This study did not generate new unique reagents.

Data and code availability

All data needed to evaluate the conclusions in the paper are present in the paper and/or the supplemental information.

Additional data related to this paper may be requested from the authors.

ACKNOWLEDGMENTS

This work was financially supported by the National Natural Science Foundation of China (grant nos. T2188101, 52021006, and 52302034), the Ministry of Science and Technology (China) of China (2022YFA1203302, 2022YFA1203304, and 2018YFA0703502), the Strategic Priority Research Program of CAS (XDB36030100), the Beijing National Laboratory for Molecular Sciences (BNLMS-CXTD-202001), and the Shenzhen Science and Technology Innovation Commission (KQTD20221101115627004). X.G. thanks the Fundamental Research for the Central Universities, Peking University.

AUTHOR CONTRIBUTIONS

X.G., J.L., Q.G., H.T., and Y.C. conceived and designed the experiments. J.L., Q.G., Z.Z., and H.T. performed the synthesis of samples. X.X. performed the theoretical simulations. J.L., Q.G., H.T., X.G., Z.D., and H.H. performed the data analysis. J.L. drafted the manuscript, and X.G., H.H., Q.G., J. Zhang, Y.C., J. Zheng, and K.J. revised it. All authors commented on the manuscript.

DECLARATION OF INTERESTS

The authors declare no conflicts of interest.

SUPPLEMENTAL INFORMATION

Supplemental information can be found online at https://doi.org/10.1016/j.matt.2025.102427.

Received: March 11, 2025 Revised: June 9, 2025 Accepted: August 15, 2025 Published: September 16, 2025

REFERENCES

- Yang, Y., Zhu, D., Yan, W., Agarwal, A., Zheng, M., Joannopoulos, J.D., Lalanne, P., Christensen, T., Berggren, K.K., and Soljačić, M. (2019). A general theoretical and experimental framework for nanoscale electromagnetism. Nature 576, 248–252. https://doi.org/10.1038/s41586-019-1803-1.
- Brunner, D.O., De Zanche, N., Fröhlich, J., Paska, J., and Pruessmann, K. P. (2009). Travelling-wave nuclear magnetic resonance. Nature 457, 994–998. https://doi.org/10.1038/nature07752.
- Zhou, X., Min, P., Liu, Y., Jin, M., Yu, Z.-Z., and Zhang, H.-B. (2024). Insulating electromagnetic-shielding silicone compound enables direct

- potting electronics. Science 385, 1205–1210. https://doi.org/10.1126/science.adp6581.
- Lv, H., Yang, Z., Wang, P.L., Ji, G., Song, J., Zheng, L., Zeng, H., and Xu, Z.J. (2018). A Voltage-Boosting Strategy Enabling a Low-Frequency, Flexible Electromagnetic Wave Absorption Device. Adv. Mater. 30, 1706343. https://doi.org/10.1002/adma.201706343.
- Shahzad, F., Alhabeb, M., Hatter, C.B., Anasori, B., Man Hong, S., Koo, C.M., and Gogotsi, Y. (2016). Electromagnetic interference shielding with 2D transition metal carbides (MXenes). Science 353, 1137–1140. https://doi.org/10.1126/science.aag2421.
- Cao, W., Li, X., Chen, Y., Jin, L., Guo, R., Song, N., Sun, S., and Ding, P. (2025). Boosting the Intelligent Development of Electromagnetic Shielding Polymer Composites by Expert Knowledge. Adv. Funct. Mater. 35, 2406738. https://doi.org/10.1002/adfm.202406738.
- Li, W., Zhou, T., Zhang, Z., Li, L., Lian, W., Wang, Y., Lu, J., Yan, J., Wang, H., Wei, L., and Cheng, Q. (2024). Ultrastrong MXene film induced by sequential bridging with liquid metal. Science 385, 62–68. https://doi. org/10.1126/science.ado4257.
- Zhou, M., Yu, Z., Yan, Q., and Zhang, X. (2025). Asymmetric Structural Design for Absorption-Dominated Electromagnetic Interference Shielding Composites. Adv. Funct. Mater. 35, 2423884. https://doi.org/10.1002/adfm.202423884.
- Zhou, M., Zhang, S., and Zhang, X. (2024). Double-layered chitosan aerogel/MXene film composites with asymmetric structure for absorptiondominated electromagnetic interference shielding and solar-driven interfacial evaporation. Adv. Compos. Hybrid Mater. 8, 44. https://doi.org/ 10.1007/s42114-024-01144-6.
- Zhuang, Z., Chen, H., and Li, C. (2023). Robust Pristine MXene Films with Superhigh Electromagnetic Interference Shielding Effectiveness via Spatially Confined Evaporation. ACS Nano 17, 10628–10636. https://doi. org/10.1021/acsnano.3c01697.
- Hashemi, S.A., Ghaffarkhah, A., Hosseini, E., Bahrani, S., Najmi, P., Omidifar, N., Mousavi, S.M., Amini, M., Ghaedi, M., Ramakrishna, S., and Arjmand, M. (2022). Recent progress on hybrid fibrous electromagnetic shields: Key protectors of living species against electromagnetic radiation. Matter 5, 3807–3868. https://doi.org/10.1016/j.matt.2022.09.012.
- Zhao, Z., Song, X., Zhang, Y., Zeng, B., Wu, H., and Guo, S. (2024). Bio-mineralization-Inspired Copper Sulfide Decorated Aramid Textiles via In Situ Anchoring toward Versatile Wearable Thermal Management. Small 20, e2307873. https://doi.org/10.1002/smll.202307873.
- Zhou, M., Zhang, S., Zhang, L., Chen, Y., Sheng, X., and Zhang, X. (2025). Integration of MXene and polymer: Unlocking the full potential of multifunctional composites for electromagnetic interference shielding. J. Mater. Sci. Technol. 226, 12–35. https://doi.org/10.1016/j.jmst.2024. 12.011.
- Men, Q., Wang, S., Yan, Z., Zhao, B., Guan, L., Chen, G., Guo, X., Zhang, R., and Che, R. (2022). Iron-encapsulated CNTs on carbon fiber with highperformance EMI shielding and electrocatalytic activity. Adv. Compos. Hybrid Mater. 5, 2429–2439. https://doi.org/10.1007/s42114-022-00457-8.
- Liu, L.-X., Chen, W., Zhang, H.-B., Wang, Q.-W., Guan, F., and Yu, Z.-Z. (2019). Flexible and Multifunctional Silk Textiles with Biomimetic Leaf-Like MXene/Silver Nanowire Nanostructures for Electromagnetic Interference Shielding, Humidity Monitoring, and Self-Derived Hydrophobicity. Adv. Funct. Mater. 29, 1905197. https://doi.org/10.1002/adfm.201905197.
- Xie, Y., Liu, S., Huang, K., Chen, B., Shi, P., Chen, Z., Liu, B., Liu, K., Wu, Z., Chen, K., et al. (2022). Ultra-Broadband Strong Electromagnetic Interference Shielding with Ferromagnetic Graphene Quartz Fabric. Adv. Mater. 34, 2202982. https://doi.org/10.1002/adma.202202982.
- Jia, L.-C., Xu, L., Ren, F., Ren, P.-G., Yan, D.-X., and Li, Z.-M. (2019).
 Stretchable and durable conductive fabric for ultrahigh performance electromagnetic interference shielding. Carbon 144, 101–108. https://doi.org/10.1016/j.carbon.2018.12.034.



- Guo, Q., Tian, H., Cheng, Y., Wang, S., Li, Z., Hao, H., Liu, J., Jiao, K., Gao, X., and Zhang, J. (2024). Structural–Functional Integrated Graphene-Skinned Aramid Fibers for Electromagnetic Interference Shielding. ACS Nano 18, 33566–33575. https://doi.org/10.1021/acsnano.4c11782.
- Chai, J., Wang, G., Wang, G., Shao, R., Zhao, J., Zhao, G., and Park, C.B. (2024). Porous and Conductive Fiber Woven Textile for Multi-Functional Protection, Personal Warmth, and Intelligent Motion/Temperature Perception. Adv. Funct. Mater. 35, 2416428. https://doi.org/10.1002/adfm. 202416428.
- Wang, Z., Cai, G., Xia, Y., Li, P., Shi, S., Wang, B., Gao, W., Liu, Y., Xu, Z., and Gao, C. (2024). Highly conductive graphene fiber textile for electromagnetic interference shielding. Carbon 222, 118996. https://doi.org/10. 1016/j.carbon.2024.118996.
- Ming, X., Wei, A., Liu, Y., Peng, L., Li, P., Wang, J., Liu, S., Fang, W., Wang, Z., Peng, H., et al. (2022). 2D-Topology-Seeded Graphitization for Highly Thermally Conductive Carbon Fibers. Adv. Mater. 34, 2201867. https://doi.org/10.1002/adma.202201867.
- Kashani, H., Giroux, M., Johnson, I., Han, J., Wang, C., and Chen, M. (2019). Unprecedented Electromagnetic Interference Shielding from Three-Dimensional Bi-continuous Nanoporous Graphene. Matter 1, 1077–1087. https://doi.org/10.1016/j.matt.2019.07.021.
- Guan, Q.-F., Han, Z.-M., Yang, K.-P., Yang, H.-B., Ling, Z.-C., Yin, C.-H., and Yu, S.-H. (2021). Sustainable Double-Network Structural Materials for Electromagnetic Shielding. Nano Lett. 21, 2532–2537. https://doi.org/10. 1021/acs.nanolett.0c05081.
- Wen, Y., Jian, M., Huang, J., Luo, J., Qian, L., and Zhang, J. (2022). Carbonene Fibers: Toward Next-Generation Fiber Materials. Nano Lett. 22, 6035–6047. https://doi.org/10.1021/acs.nanolett.1c04878.
- Zhou, G., Wang, Y.-Q., Byun, J.-H., Yi, J.-W., Yoon, S.-S., Cha, H.-J., Lee, J.-U., Oh, Y., Jung, B.-M., Moon, H.-J., and Chou, T.-W. (2015). High-Strength Single-Walled Carbon Nanotube/Permalloy Nanoparticle/Poly (vinyl alcohol) Multifunctional Nanocomposite Fiber. ACS Nano 9, 11414–11421. https://doi.org/10.1021/acsnano.5b05404.
- Luo, J., Wen, Y., Li, T., Jia, X., Lei, X., Zhang, Z., Xiao, Z., Wu, X., Gao, Z., Gao, E., et al. (2024). High Interfacial Shear Strength and High Tensile Strength in Heterocyclic Aramid Fibers with Improved Interchain Interaction. Adv. Funct. Mater. 34, 2310008. https://doi.org/10.1002/adfm. 202310008
- Xie, L., Min, P., Ye, L., He, P., Yin, G., Jin, M., Zhang, H.-B., and Yu, Z.-Z. (2024). Interfacial enhancement enables highly conductive reduced graphene oxide-based yarns for efficient electromagnetic interference shielding and thermal regulation. Carbon 230, 119655. https://doi.org/10.1016/j.carbon.2024.119655.
- Cao, C., Peng, J., Liang, X., Saiz, E., Wolf, S.E., Wagner, H.D., Jiang, L., and Cheng, Q. (2021). Strong, conductive aramid fiber functionalized by graphene. Compos. Part A: Appl. S. 140, 106161. https://doi.org/10. 1016/j.compositesa.2020.106161.
- Ke, F., Song, F., Zhang, H., Xu, J., Wang, H., and Chen, Y. (2020). Layer-by-layer assembly for all-graphene coated conductive fibers toward superior temperature sensitivity and humidity independence. Compos. Part B: Eng. 200, 108253. https://doi.org/10.1016/j.compositesb.2020.108253.
- Li, X., Zong, L., Wu, X., You, J., Li, M., and Li, C. (2018). Biomimetic engineering of spider silk fibres with graphene for electric devices with humidity and motion sensitivity. J. Mater. Chem. C 6, 3212–3219. https://doi.org/10.1039/c8tc00265g.

- Lv, J., Cheng, Z., Wu, H., He, T., Qin, J., and Liu, X. (2020). In-situ polymerization and covalent modification on aramid fiber surface via direct fluorination for interfacial enhancement. Compos. Part B: Eng. 182, 107608. https://doi.org/10.1016/j.compositesb.2019.107608.
- Punckt, C., Muckel, F., Wolff, S., Aksay, I.A., Chavarin, C.A., Bacher, G., and Mertin, W. (2013). The effect of degree of reduction on the electrical properties of functionalized graphene sheets. Appl. Phys. Lett. 102, 023114. https://doi.org/10.1063/1.4775582.
- Parvez, K., Wu, Z.-S., Li, R., Liu, X., Graf, R., Feng, X., and Müllen, K. (2014). Exfoliation of Graphite into Graphene in Aqueous Solutions of Inorganic Salts. J. Am. Chem. Soc. 136, 6083–6091. https://doi.org/10.1021/ja5017156.
- Gao, Z., Song, Q., Xiao, Z., Li, Z., Li, T., Luo, J., Wang, S., Zhou, W., Li, L., Yu, J., and Zhang, J. (2023). Submicron-Sized, High Crystalline Graphene-Reinforced Meta-Aramid Fibers with Enhanced Tensile Strength. Acta Phys. Chim. Sin. 0, 202307046. https://doi.org/10.3866/pku.Whxb20 2307046
- Ferrari, A.C., Meyer, J.C., Scardaci, V., Casiraghi, C., Lazzeri, M., Mauri, F., Piscanec, S., Jiang, D., Novoselov, K.S., Roth, S., and Geim, A.K. (2006). Raman Spectrum of Graphene and Graphene Layers. Phys. Rev. Lett. 97, 187401. https://doi.org/10.1103/PhysRevLett.97.187401.
- Yuan, G., Lin, D., Wang, Y., Huang, X., Chen, W., Xie, X., Zong, J., Yuan, Q.-Q., Zheng, H., Wang, D., et al. (2020). Proton-assisted growth of ultra-flat graphene films. Nature 577, 204–208. https://doi.org/10.1038/s41586-019-1870-3.
- Yang, Y., Zhao, X., Zhang, C., Tong, Y., Hu, J., Zhang, H., Yang, M., Ye, X., Wang, S., Sun, Z., et al. (2020). Ultraflexible, Degradable Organic Synaptic Transistors Based on Natural Polysaccharides for Neuromorphic Applications. Adv. Funct. Mater. 30, 2006271. https://doi.org/10.1002/adfm. 202006271.
- Cheng, M., Ying, M., Zhao, R., Ji, L., Li, H., Liu, X., Zhang, J., Li, Y., Dong, X., and Zhang, X. (2022). Transparent and Flexible Electromagnetic Interference Shielding Materials by Constructing Sandwich AgNW@MXene/Wood Composites. ACS Nano 16, 16996–17007. https://doi.org/10.1021/acsnano.2c07111.
- Kim, K.H., Oh, Y., and Islam, M.F. (2012). Graphene coating makes carbon nanotube aerogels superelastic and resistant to fatigue. Nat. Nanotechnol. 7, 562–566. https://doi.org/10.1038/nnano.2012.118.
- Shin, M.K., Lee, B., Kim, S.H., Lee, J.A., Spinks, G.M., Gambhir, S., Wallace, G.G., Kozlov, M.E., Baughman, R.H., and Kim, S.J. (2012). Synergistic toughening of composite fibres by self-alignment of reduced graphene oxide and carbon nanotubes. Nat. Commun. 3. https://doi.org/10.1038/ncomms1661
- Lu, Y., Zhang, S., He, M., Wei, L., Chen, Y., and Liu, R. (2021). 3D cross-linked graphene or/and MXene based nanomaterials for electromagnetic wave absorbing and shielding. Carbon 178, 413–435. https://doi.org/10.1016/j.carbon.2021.01.161.
- Zhou, M., Hu, Y., Yan, Z., and Fu, H. (2024). Flexible MXene-based Janus film with superior heat dissipation capability for ultra-efficient electromagnetic interference shielding and Joule heating. Carbon 219, 118835. https://doi.org/10.1016/j.carbon.2024.118835.
- Zhang, Z., Jia, X., Li, C., Li, L., Wen, Y., Gao, Z., Zhang, J., Gao, E., Jiao, K., and Zhang, J. (2023). Simultaneously enhanced interfacial shear strength and tensile strength of heterocyclic aramid fiber by graphene oxide. Nano Res. 16, 12286–12293. https://doi.org/10.1007/s12274-023-5904-7.